

Lorentz Factor Constraint from the very early external shock of the gamma-ray burst ejecta

Yuan-Chuan Zou^{1,2}, and Tsvi Piran¹ \star

¹*The Racah Institute of Physics, Hebrew University, Jerusalem 91904, Israel*

²*School of Physics, Huazhong University of Science and Technology, Wuhan 430074, China*

31 October 2018

ABSTRACT

While it is generally agreed that the emitting regions in Gamma-Ray Bursts (GRBs) move ultra relativistically towards the observer, different estimates of the initial Lorentz factors, Γ_0 , lead to different, at times conflicting estimates. We show here that the quiet periods in which the signals goes down below the instrumental thresholds, put strong upper limits on the values of Γ_0 . According to the standard internal-external shocks model an external shock should develop during the prompt stage. This external shock radiates in the hard X-rays to soft gamma-rays bands and this emission should be seen as a smooth background signal. The observed deep minima indicate that this contribution is negligible. This limits, in turn, Γ_0 . We obtain upper limits on Γ_0 for several bursts with typical values around hundreds. We compare these values with those obtained by the other methods, which typically yield lower limits. The results are marginally consistent leaving only a narrow range of allowed values for Γ_0 .

Key words: gamma rays: bursts—radiation mechanism: nonthermal

1 INTRODUCTION

The combination of fast variability and a non-thermal spectrum lead to the well known “compactness problem” and indicates that the emitting region of GRBs move relativistically towards the observers (Ruderman 1975) (or that they are extremely nearby). With the realization, in the early nineties, that GRBs are cosmological and the development of the fireball model, relativistic motion became an essential ingredient of GRB modeling. Relativistic motion was confirmed, first by observations of scintillations at the radio afterglow of GRB 970508 (Goodman 1997; Waxman, Kulkarni & Frail 1998), later by afterglow modeling (Sari, Piran & Narayan 1998; van Paradijs, Kouveliotou & Wijers 2000; Penaitescu & Kumar 2002) and finally in direct observations of superluminal motion in the afterglow of GRB 030329 (Taylor et al. 2004; Oren, Nakar & Piran 2004).

These observations were all done during the afterglow phase in which the ejected material has already been slowed down by its interaction with the surrounding material and the typical Lorentz factor was of order 5 or less. However, the compactness problem indicates that the initial Lorentz factor, Γ_0 , with which the jet was ejected from the inner engine and with which it was moving during the prompt GRB phase, was much larger.

In spite of this progress Γ_0 , which is crucial to understand the underline physics both of the inner engine and of the emission process is still unknown. Several methods have been proposed to estimate it. The methods vary in complexity and in robustness and

depend on different details of the “internal-external” shocks model and/or on the development of an forward-reverse shocks system during the early phase of the afterglow:

- The simplest, most direct and robust method uses the compactness problem: The optical depth for high energy photons (\sim GeV) to escape from the emitting region without being annihilated by softer γ -rays (sub-MeV) should be less than unity. This leads to a lower limit on the initial Lorentz factor (Fenimore, Epstein & Ho 1993; Piran 1995; Woods & Loeb 1995; Baring & Harding 1997; Lithwick & Sari 2001). It can be used to set an exact value for the Lorentz factor if an upper energy cutoff is observed. However, this was not seen so far. Using this method, Lithwick & Sari (2001) obtained lower limits of Γ_0 (typically of order of several hundred) for several bursts.

- Within the external shocks scenario the peak of the light curve corresponds to the decelerating time of the ejecta (Mészáros & Rees 1997; Sari & Piran 1999a,b; Kobayashi 2000). Observations of this peak provide, therefore, a way to estimate Γ_0 . Rykoff et al. (2009) constrained Γ_0 using this method for several bursts whose prompt optical emission was observed by ROTSE-III. Zhang et al. (2006) argued that the deceleration time should be prior to the shallow decay phase, and used this to obtain lower limits \sim 100 for several bursts.

- Comparison of the early X-ray and optical emission (that arise from a reverse-forward shock system) enables us to estimate the Lorentz factor by fitting parameters of the emitting regions (Sari & Piran 1999a; Zhang, Kobayashi & Mészáros 2003). As an example, using this method Sari & Piran (1999a) constrained Γ_0 of GRB 990123 to be \sim 200. Molinari (2007) and Jin & Fan (2007)

\star Email: zouyc@hust.edu.cn (YCZ) and tsvi@phys.huji.ac.il (TP)

estimated using the early optical afterglow, Γ_0 , to be ~ 400 for both GRB 060418 and GRB 060607A. Recently, Xue, Fan & Wei (2009) used the reverse-forward shock model to determine the initial Lorentz factor for several well observed bursts and obtained typical values of 300.

- Thermal emission escapes from the fireball’s photospheric when it becomes optically thin. The observations of a thermal component would allow us, therefore, to infer the Lorentz factor at this time (Nakar, Piran & Sari 2005; Pe’er et al. 2007). Assuming that such a component was indeed observed and using this method Pe’er et al. (2007) estimated Γ_0 to be hundreds.

In this work we propose yet another method to estimate Γ_0 . We work within the “internal-external” shocks scenario according to which internal shocks that arise due to collisions of the ejected shells within the relativistic outflow produce the observed prompt gamma-rays, while the interaction of the merged shells with the surrounding medium produces the afterglow (see Piran 2005, for a review). However, an external shock begins to develop even during the prompt phase. It is caused by the outermost shell that sweeps up the external medium. This external shock radiates and produces an underlying smooth component. Usually, this extra component will be sub-dominant when the internal shocks emission is strong. However, as this emission is not observed even during troughs of the light curves it must be weaker than the detection threshold in cases when a deep minimum in the light curve is observed. For example, *Swift* BAT has a sensitivity limit of $\sim 10^{-8}$ ergs cm $^{-2}$ s $^{-1}$ (Gehrels et al. 2004) (corresponding to $f_{\nu, \text{lim}} \sim 4 \times 10^{-28}$ ergs cm $^{-2}$ s $^{-1}$ Hz $^{-1}$). We show here that the strength of the early forward shock emission depends sensitively on the Lorentz factor at this stage (which is roughly the initial one). Using this we set upper limits on the initial Lorentz factor for variant bursts.

We derive the radiation flux density from the forward shock, and the resulting constraint on Γ_0 in section 2. We examine other methods for constraining Γ_0 in section 3. We calculate the constraints for several selected individual bursts using three methods in section 4 and discuss the implications of the results in section 5.

2 MODEL

Our model is based on a basic ingredient of the “internal-external shocks model”. Within this model, while internal shocks are going on producing the prompt gamma-rays the outermost shell that is at the front of the ejecta begins interacting with the surrounding matter and an reverse-forward shocks system develops (Sari & Piran 1995; Zhang, Kobayashi & Mészáros 2003; Nakar & Piran 2004). The reverse shock propagates back into the front of the ejecta and the external shock propagates into the surrounding matter. We consider here the emission from this very early reverse-forward shocks system. The contribution of the forward shock should appear in soft gamma-rays as a smooth and continuous emission with an increasing signal. However, in many cases the observed signal decreases to very low values, which can be even below the detection limit of the observing instrument. We use this to constrain the initial Lorentz factor. Depending on the environment, we consider two cases: interstellar medium (ISM) and a wind.

2.1 An ISM

The reverse shock can be relativistic (RRS) or Newtonian (NRS) depending on a density ratio between the ejecta and the surrounding

matter. The relevant case depends on the parameter (Sari & Piran 1995; Nakar & Piran 2004):

$$\xi \equiv \left(\frac{l}{\Delta_0} \right)^{1/2} \Gamma_0^{-4/3} \simeq 34 n_0^{-1/6} \Delta_{0,10}^{-1/2} \eta_2^{-4/3} E_{53}^{1/6}, \quad (1)$$

where $l \equiv (3E/4\pi n m_p c^2)^{1/3}$ is the Sedov length, Γ_0 is the initial Lorentz factor of the merged shell, which is also the Lorentz factor of the prompt gamma-ray emitting region, Δ_0 is the initial width of the shell, which is related to the duration of the pulse by $\delta t \sim \Delta_0/(2c) \sim 0.1$ s (Wu et al. 2003), E is the isotropic kinetic energy, n is the matter number density, and m_p is the proton rest mass. The conventional notation $Q = Q_x \times 10^x$ is used throughout this paper. $\xi < 1$ leads to RRS, while $\xi > 1$ corresponds to NRS.

Typical values of the parameters have been used in eq. (1). Unless η or Δ are very large, $\xi \gg 1$, so we only consider the NRS case. As the Newtonian reverse shock radiates near the optical band, the main contribution to the X-ray to soft gamma-ray emission arises from the forward shock, which we examine now.

The deceleration radius for the outermost shell is

$$R_d = \left(\frac{3E_0}{4\pi n \Gamma_0^2 m_p c^2} \right)^{1/3} = 1.2 \times 10^{17} E_{53}^{1/3} \Gamma_{0,2}^{-2/3} n_0^{-1/3} \text{ cm} \quad (2)$$

Consequently, the deceleration time is $t_{\oplus, d} = \frac{R_d}{2\eta^2 c} \simeq 1.9 \times 10^2 (1+z) E_{53}^{1/3} \Gamma_{0,2}^{-2/3} n_0^{-1/3}$ s, which is much longer than the time of the first minimum in which we are interested. So we can consider the scaling-laws for the very early external shock before it has been decelerated. During this phase the shell coasts with a constant Lorentz factor Γ_0 , collecting the medium to radiate X-rays and the shock accelerated electrons are cooled mainly via synchrotron emission.

Following Sari, Piran & Narayan (1998) (see also in e.g. Nakar & Piran 2004; Zou, Wu & Dai 2005), we calculate the dynamics and radiation from the forward shock. The internal energy density of the forward shocked material is $e = 4\eta^2 m_p c^2 n \simeq 60 n_0 \Gamma_{0,2}^2 \text{ erg cm}^{-3}$, the magnetic field in the comoving frame is $B = \sqrt{8\pi e_B e} \simeq 12 n_0^{1/2} \epsilon_{B,-1}^{1/2} \Gamma_{0,2} \text{ Gauss}$, where ϵ_B is the equipartition factor for the magnetic energy density. The peak spectral power is $P_{\nu, \text{max}} = (1+z) \sigma_T m_e c^2 \Gamma_0 B / (3q_e) \simeq 4.7 \times 10^{-19} (1+z) n_0^{1/2} \epsilon_{B,-1}^{1/2} \Gamma_{0,2}^2 \text{ erg Hz}^{-1} \text{ s}^{-1}$, where σ_T is the Thomson cross section, q_e is the electron charge. The peak observed flux density is then $f_{\nu, \text{max}} = N_e P_{\nu, \text{max}} / (4\pi D^2) \simeq 3.4 \times 10^{-31} D_{28}^{-2} (1+z)^{-2} n_0^{3/2} t_{\oplus}^3 \epsilon_{B,-1}^{3/2} \Gamma_{0,2}^8 \text{ erg cm}^{-2} \text{ Hz}^{-1} \text{ s}^{-1}$, where N_e is the total number of emitting electrons, and D is the luminosity distance. The synchrotron cooling Lorentz factor is $\gamma_c = 6\pi m_e c / (\sigma_T B^2 t_{co}) \simeq 2.6 \times 10^4 n_0^{-1} \Gamma_{0,2}^{-3} (1+z) t_{\oplus}^{-1} (1+Y)^{-1} \epsilon_{B,-1}^{-1}$ (where t_{co} is the comoving time scale and Y is the Compton parameter for synchrotron self-Compton scattering). This corresponds to the cooling frequency $\nu_c = (1+z)^{-1} \frac{\Gamma_0 \gamma_c^2 q_e B}{2\pi m_e c} \simeq 2.3 \times 10^{18} (1+z) n_0^{-3/2} t_{\oplus}^{-2} \epsilon_{B,-1}^{-3/2} \Gamma_{0,2}^{-4} \text{ Hz}$. The typical Lorentz factor of the electrons is $\gamma_m = \frac{p-2}{p-1} \frac{\epsilon_e e}{n_2 m_e c^2} \simeq 2.0 \times 10^5 \zeta_1 \Gamma_{0,2} \epsilon_{e,-1/2}$, and the typical synchrotron frequency is $\nu_m = (1+z)^{-1} \frac{\Gamma_0 \gamma_m^2 q_e B}{2\pi m_e c} \simeq 1.3 \times 10^{18} (1+z)^{-1} n_0^{1/2} \epsilon_{B,-1}^2 \epsilon_{e,-0.5}^2 \Gamma_{0,2}^4 \zeta_{1/3}^2 \text{ Hz}$, where $\zeta = 3 \frac{p-2}{p-1}$, and p is the index of power law distributed electrons. The Synchrotron-self absorption frequency is $\nu_a \sim 2.8 \times 10^8 (1+z)^{-1/5} n_0^{9/5} t_{\oplus}^{8/5} \epsilon_{B,-1}^{6/5} \Gamma_{0,2}^{28/5} \text{ Hz}$ for $\nu_a < \nu_c < \nu_m$ and $\nu_a \sim 4.6 \times$

$10^8 (1+z)^{-\frac{8}{5}} n_0^{\frac{4}{5}} t_{\oplus}^{\frac{3}{5}} \epsilon_{B,-1}^{\frac{1}{5}} \epsilon_{e,-0.5}^{-1} \Gamma_{0,2}^{\frac{8}{5}} \text{ Hz}$ for $\nu_a < \nu_m < \nu_c$, which are always well below ν_m and ν_c .

Collecting the above expressions, the observed flux density f_ν is:

$$f_\nu = 2 \times 10^{-33} \Gamma_{0,2}^9 D_{28}^{-2} (1+z)^{-\frac{9}{4}} n_0^{\frac{9}{8}} t_{\oplus}^2 \epsilon_{B,-1}^{\frac{1}{8}} \epsilon_{e,-\frac{1}{2}}^{\frac{3}{2}} \nu_{20}^{-\frac{5}{4}} (1+Y)^{-1} \text{ erg cm}^{-2} \text{ Hz}^{-1} \text{ s}^{-1} \quad (3)$$

for $p = 2.5^1$ and $\nu > (\nu_a, \nu_c, \nu_m)$. One can see that f_ν depends very sensitively on the initial Lorentz factor Γ_0 . This is partially because of the number of emitting electrons N_e , for $N_e = 4\pi/3R^3 n \propto \Gamma_0^6 t_{\oplus}^3 n$, behaves like Γ_0^6 .

For different parameters, especially for different values of Γ_0 , ν may be either greater or smaller than ν_m or ν_c . Figure 1 shows rough spectra and the relations between the different frequencies for 3 different values of Γ_0 . Even though the observed frequency is not always larger than ν_c and ν_m , it is never significantly smaller. Therefore, equation (3) is roughly acceptable for the whole range of parameters of interest. For simplicity, we use only this equation in the following discussion.

If the observed flux density immediately after the first GRB pulse is $f_{\nu,C}$. The emission of the early external shock should not exceed this value, requiring $f_\nu \leq f_{\nu,C}$. In other cases, there is no signal immediately after the first pulse, when $f_\nu < f_{\nu,lim}$, where $f_{\nu,lim}$ is the limiting flux density of the observing instrument. We use $f_{\nu,lim}$ to represent both quantities in the following. Using $f_{\nu,lim} = 10^{-28} \text{ erg cm}^{-2} \text{ Hz}^{-1} \text{ s}^{-1}$, this inequality gives a strong constraint on Γ_0 :

$$\Gamma_0 < 340(1+z)^{\frac{1}{4}} f_{\nu,lim,-28}^{\frac{1}{9}} D_{28}^{\frac{2}{9}} n_0^{-\frac{1}{8}} \epsilon_{e,-\frac{1}{2}}^{-\frac{1}{6}} \epsilon_{B,-1}^{-\frac{1}{72}} \nu_{20}^{\frac{5}{36}} t_{\oplus}^{-\frac{2}{9}} (1+Y)^{\frac{1}{9}}, \quad (4)$$

Note that the limit practically depends rather weakly on all the other parameters. For completeness, we also present the expression for a general p :

$$\Gamma_0 < 340 \times 2.4^{-\frac{p-2.5}{9(p+2)}} \left[f_{\nu,lim,-28} (1+z)^{\frac{p+2}{2}} D_{28}^2 n_0^{-\frac{p+2}{4}} \epsilon_{e,-\frac{1}{2}}^{-(p-1)} \epsilon_{B,-1}^{-\frac{p-2}{4}} \nu_{20}^{\frac{p}{2}} t_{\oplus}^{-2} [3(p-2)/(p-1)]^{-(p-1)} (1+Y)^{\frac{1}{2p+4}} \right] \quad (5)$$

As the value of p ranges between 2 and 3 generally, and as the overall expression depends on $\frac{1}{2p+4}$, Γ_0 is weakly dependent on the other parameters for a general p .

2.2 A wind environment

For a wind environment, the distinction between RRS and NRS depends on (Wu et al. 2003)

$$\xi \equiv \left(\frac{l}{\Delta_0} \right)^{1/2} \Gamma_0^{-2} \simeq 23 E_{53}^{1/2} A_{\star}^{-1/2} \Delta_{0,10}^{-1/2} \Gamma_{0,2}^{-2} \quad (6)$$

¹ Note that for simplicity, the above relations are given for $p = 2.5$. For other values of p , the indices will change accordingly but not too much. For example, if $p = 2.2$, the scaling law is $f_\nu \propto \Gamma_0^{42/5}$ rather than $\propto \Gamma_0^9$. As the flux density in the gamma-ray band is $f_{\nu,max}(\nu_c/\nu_m)^{-(p-1)/2}(\nu/\nu_c)^{-p/2}$ or $f_{\nu,max}(\nu_c/\nu_m)^{-(p-1)/2}(\nu/\nu_c)^{-p/2}$, which is lower with higher value of p . Therefore, the choice of $p = 2.5$ is conservative when evaluating the minimal flux density, as the usual value of p is around 2.2 (Achterberg et al. 2001). Furthermore, the value of p in the range of [2,3] doesn't change the emission much. See also eq. (5) for a general p .

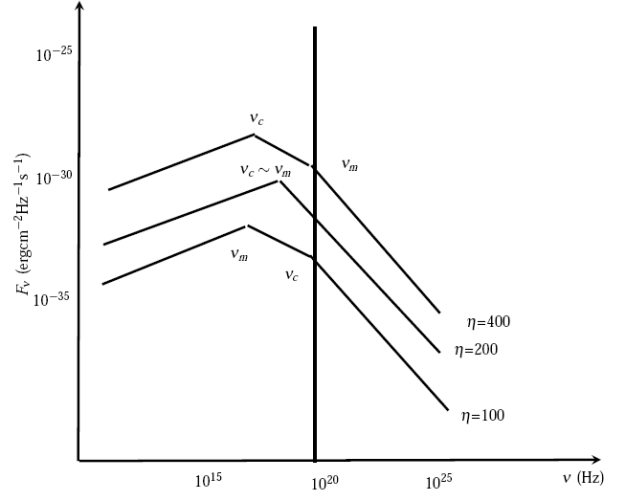


Figure 1. The sketched synchrotron spectra of the forward shock emission before the deceleration. The lines indicate for $\Gamma_0 = 400, 200$ and 100 from top to down respectively.

where the Sedov length in a wind case is $l \equiv E_0/(4\pi A m_p c^2)$, A is the wind parameter satisfying $n(r) = Ar^{-2}$, and $A = 3 \times 10^{35} A_{\star} \text{ cm}^{-1}$. For typical parameters the NRS case is also most likely. The deceleration radius is

$$R_d = \frac{E_0}{4\pi A \Gamma_0^2 m_p c^2} = 1.8 \times 10^{16} E_{53} \Gamma_{0,2}^{-2} A_{\star,-1}^{-1} \text{ cm}, \quad (7)$$

and the corresponding deceleration time is $t_{\oplus,d} = 30(1+z) E_{53} \Gamma_{0,2}^{-4} A_{\star,-1}^{-1} \text{ sec}$, which is also longer than a typical first pulse. The observed flux density of the forward shock before deceleration is:

$$f_\nu \sim 2 \times 10^{-27} \Gamma_{0,2}^{\frac{9}{2}} D_{28}^{-2} A_{\star,-1}^{\frac{9}{8}} t_{\oplus}^{-\frac{1}{4}} \epsilon_{B,-1}^{\frac{1}{8}} \epsilon_{e,-\frac{1}{2}}^{\frac{3}{2}} \nu_{20}^{-\frac{5}{4}} (1+Y)^{-1} \text{ erg cm}^{-2} \text{ Hz}^{-1} \text{ s}^{-1} \quad (8)$$

in the case $\nu > (\nu_m, \nu_c, \nu_a)$ (see Zou, Wu & Dai (2005) for other cases). As the wind density is much higher than the ISM density, the flux density is much higher than the one expected for an ISM (given by eq. (3)). For the typical parameter $A_{\star} = 0.1$, the number density at a given radius $R = 2\Gamma_0^2 ct_{\oplus} \sim 6 \times 10^{14} \Gamma_{0,2}^2 t_{\oplus} \text{ cm}$ is about 10^6 larger than the ISM, and consequently, the flux density is about 10^6 stronger, as it is proportional to $n^{9/8}$. For $p = 2.5$, the initial Lorentz factor can be expressed as

$$\Gamma_0 < 50 f_{\nu,lim,-28}^{\frac{2}{9}} D_{28}^{\frac{4}{9}} A_{\star,-1}^{-\frac{1}{4}} \epsilon_{e,-\frac{1}{2}}^{-\frac{1}{3}} \epsilon_{B,-1}^{-\frac{1}{36}} \nu_{20}^{\frac{5}{18}} t_{\oplus}^{\frac{1}{18}} (1+Y)^{\frac{2}{9}}. \quad (9)$$

The limit is even stronger than the one obtained in ISM case. This is essentially because of the denser medium for the typical wind parameter. However, the density profile is uncertain at small values of r (that are relevant at this stage) and it is not clear if this limit is valid. In any case, this is a strong argument against very dense environment near GRBs.

3 OTHER CONSTRAINTS

As mentioned earlier several other methods to constrain the initial Lorentz factor have been suggested. We compare the constraints

obtained using the different methods to show the consistency of the overall model. As most other methods give lower limits, combined with ours, we obtain a overall stronger constraint.

3.1 Compactness and the optical depth for pair production

Observations of high energy photons from a GRB imply that the emitting region is optically thin for pair production of these high energy photons with the lower energy sub-MeV gamma-rays. This leads to a limit (Lithwick & Sari 2001) (denoted limit A)

$$\Gamma_0 > \hat{\tau}^{1/(2\beta+2)} (E_{\max}/m_e c^2)^{(\beta-1)/(2\beta+2)} (1+z)^{\beta-1/\beta+1}, \quad (10)$$

where β is the photon spectral index ($f E^{-\beta} \text{cm}^{-2} \text{s}^{-1} \text{erg}^{-1}$), E_{\max} is the maximal energy of the observed high energy photons, and $\hat{\tau}$ is defined as

$$\begin{aligned} \hat{\tau} &\equiv \frac{(11/180)\sigma_T D^2 (m_e c^2)^{-\beta+1} f}{c^2 \delta T (\beta-1)} \\ &\simeq 4.3 \times 10^{10} \frac{f_1}{\beta-1} D_{28}^2 0.511^{-\beta+1} \delta T_{-1}^{-1}, \end{aligned} \quad (11)$$

where D is the luminosity distance, δT is the variability time scale of the prompt emission, and $f_1 \equiv f(\text{MeV})^{-\beta+1} \text{s}^{-1} \text{cm}^{-2}$ is the number of photons per second per square centimeter per MeV at energy of 1 MeV.

When high energy observations are not available, we can still obtain a bound by assuming that the observed higher energy spectrum at around a MeV can extend up to the energy where photons can just annihilate with themselves in the same spectral shape. This leads to another constraint (Lithwick & Sari 2001) (denoted limit B):

$$\Gamma_0 > \hat{\tau}^{1/(\beta+3)} (1+z)^{\beta-1/\beta+3}. \quad (12)$$

Typically, limit A yields a tighter constraint than limit B.

3.2 The deceleration time

The deceleration time of the external forward shock, $t_{\gamma,2}$ corresponds to the peak in the afterglow light curve. It depends weakly on the overall energy and the external density and most sensitively on the initial Lorentz factor. At the deceleration time, the Lorentz factor is a half of the initial Lorentz factor. This yields (Sari & Piran 1999b):

$$\Gamma_0 \sim 190 E_{k,52}^{1/8} n_0^{-1/8} t_{\gamma,2}^{-3/8} (1+z)^{3/8}. \quad (13)$$

where t_γ is the deceleration time, that corresponds to the peak in the afterglow light curve.

By employing an efficiency parameter $\bar{\eta} \equiv E_{\gamma,\text{iso}}/E_{k,\text{iso}}$, where $E_{k,\text{iso}}$ and $E_{\gamma,\text{iso}}$ are isotropic equivalent kinetic energy and the prompt emitted photon energy respectively, we get

$$\Gamma_0 \sim 220 E_{\gamma,\text{iso},52}^{1/8} \bar{\eta}_{-0.5}^{-1/8} n_0^{-1/8} t_{\gamma,2}^{-3/8} (1+z)^{3/8}, \quad (14)$$

For a wind environment, the initial Lorentz factor is (Panaitescu & Kumar 2000)

$$\Gamma_0 \sim 110 E_{\gamma,\text{iso},52}^{1/4} \bar{\eta}_{-0.5}^{-1/4} A_{\star,-1}^{-1/4} t_{\gamma,2}^{-1/4} (1+z)^{1/4}, \quad (15)$$

where $A_\star = 3 \times 10^{35} \text{cm}^{-2}$ is the wind parameter.

3.3 A photospheric thermal component

A thermal component, should come from the fireball's photosphere (where the optical depth is unity). Detection of such a component would enable us to determine the initial Lorentz factor using (Nakar, Piran & Sari 2005; Pe'er et al. 2007):

$$\Gamma_0 \simeq \left[(1+z)^2 D \frac{F_{\text{obs}} \sigma_T}{2m_p c^3 \mathcal{R}} \right]^{1/4}, \quad (16)$$

where $\mathcal{R} = (F_{BB}/\sigma T_{\text{obs}}^4)^{1/2}$, and F_{BB} is the thermal component emission.

3.4 The reverse-forward shocks system

During the early afterglow, the predicted reverse-forward shock may give a direct clue to determine the initial Lorentz factor, as the Lorentz factor of the unshocked ejecta (that is involved with the reverse shock) is roughly equal to the initial Lorentz factor. By fitting the early afterglow to the predictions of the reverse-forward shock model, one obtains different parameters within the shocked region including the Lorentz factor. This is the final Lorentz factor after the merging during internal shocks, which may be regarded as an average value of the initially ejected sub-shells.

We have listed several methods. However, not all are practical. Specifically, it is difficult to dig out a thermal component within the total emission as needed for the thermal component method (see however Ryde 2005). Similarly, the identification of a reverse-forward shocks system is limited and available only for a few bursts. In the following we will use only the methods in sections 3.1 (LS01A or LS01B) and 3.2 (SP99).

4 CASE STUDY AND A COMPARISON OF THE DIFFERENT METHODS

We examine some well observed bursts to see whether the different constrains on the initial Lorentz factor are consistent with each other. The new constraint described here is based on the observation of the first pulse and the following minimum. For subsequent pulses the forward shock is complicated. Therefore, the constraint is only suitable for those bursts which exhibit a short first pulse followed by a deep trough. In the following we consider only such bursts. To use the three methods, we need the bursts have the properties: (i) A GeV signals (for LS01A). (ii) A clear first pulse and a subsequent minimum (for this work, ZP09), with not long duration, otherwise, the external shock may have decelerated during the first pulse. (iii) A peak in the optical afterglow light curve (for SP99). However, it is very rare satisfying all the three requirements. Then we reduce it to any burst who has two of the above properties as the sample to examine the Γ_0 . We use typical parameters: $f_{\nu,\text{lim}} \sim 4 \times 10^{-28} \text{ergs cm}^{-2} \text{s}^{-1} \text{Hz}^{-1}$ as the detection limit if it is a *Swift* burst; $\bar{\eta} \simeq 0.3$, $n = 1 \text{cm}^{-3}$, $p = 2.5$, $\epsilon_e \simeq 0.3$, and $\epsilon_B = 0.1$ if they are not determined.

GRB 990123

GRB 990123 was located at $z = 1.60$ ($D_L = 3.7 \times 10^{28} \text{cm}$) with an isotropic equivalent energy in γ -rays $E_{\gamma,\text{iso}} \sim 3.4 \times 10^{54} \text{ergs}$ (Kulkarni et al. 1999). It has been extensively discussed. Lithwick & Sari (2001) obtained a lower limit of $\Gamma_0 \approx 150$ using

LS01A and 180 using LS01B (assuming there is a single power law in the spectrum of the high energy band).

The afterglow light curve can be fitted both by a uniform medium and a wind-type medium, with parameters $n = 0.004 \text{ cm}^{-3}$, $\epsilon_e = 0.075$, $\epsilon_B = 4 \times 10^{-4}$, for uniform medium and $A_* = 0.06$, $\epsilon_e = 0.08$, $\epsilon_B = 7 \times 10^{-5}$, for wind-type medium respectively, while the underlying physical parameters are somewhat uncertain (Panaitescu 2005). The prompt BATSE light curve shows a valley at $\sim 12 \text{ sec}$ (Galama et al. 1999). BATSE sensitivity in 50-300 keV, is $0.2 \text{ cm}^{-2} \text{ s}^{-1}$ (<http://glast.gsfc.nasa.gov/science/instruments/table1-2.html>), corresponding to a flux density of $f_{\nu,lim} \sim 1.25 \times 10^{-27} \text{ erg cm}^{-2} \text{ s}^{-1} \text{ Hz}^{-1}$. Using those parameters and equations (4) and (9), we obtain an upper limit of $\Gamma_0 < 1200$ for a uniform medium and 410 for wind-type medium by our method.

From the optical light curve (Galama et al. 1999), the decelerating time should be less than 0.1 day ($\sim 8640 \text{ s}$). (Though there were also optical observations before, they are generally considered as reverse-forward shock signals (Sari & Piran 1999a).) Using equations (14) and (15), and assuming the efficiency $\bar{\eta} = 0.3$, we obtain lower limit of 100 for uniform medium and 130 for wind-type medium respectively by method SP99.

These constraints are consistent with those obtained by light curve fitting, e.g. $\Gamma_0 = 270$ by Kobayashi (2000) and $\Gamma_0 = 1200$ by Wang, Dai & Lu (2000).

GRB 021004

GRB 021004 was observed by HETE-II, and located at redshift $z = 2.32$ ($D_L \sim 5.8 \times 10^{28} \text{ cm}$) (Fox et al. 2003). Lacking high energy data, we cannot use method LS01A. To use method LS01B, we need the spectrum of the prompt emission. However, the spectrum fitting was a single power-law with photon index $\beta \sim 1.64$ (Lamb et al. 2002). An extended single power-law with $\beta < 2$ indicates the most energy is hidden in the higher energy band and there must be a spectral break and an unknown high energy spectral index. Therefore, we cannot carry out the estimation by method LS01B neither.

The duration of the first pulse is $\sim 10 \text{ sec}$ (<http://space.mit.edu/HETE/Bursts/GRB021004/>). HETE's Detection thresholds for the French Gamma Telescope (FREGATE) is $\sim 3 \times 10^{-8} \text{ erg cm}^{-2} \text{ s}^{-1}$ (<http://space.mit.edu/HETE/fregate.html>), which corresponding to $f_{\nu,lim} \sim 1.2 \times 10^{-27} \text{ erg cm}^{-2} \text{ Hz}^{-1} \text{ s}^{-1}$ at 100 keV. The afterglow emission was fitted well by wind-type environment, with parameters $A_* = 0.6$, $E_{k,52} = 10$, $\epsilon_e = \epsilon_B = 0.1$ (Li & Chevalier 2003). Using equation (9), we obtain the upper limit of $\Gamma_0 < 210$.

From the optical light curve, which was first observed 537sec after the trigger of the burst (Fox et al. 2003), the decelerating time of the external shock should be shorter than this time. Using equation (15), we obtain (by method SP99) $\Gamma_0 > 80$.

GRB 040924

GRB 040924 was a short burst with duration $T_{90} = 2.39 \pm 0.24 \text{ s}$. It was located at $z = 0.858$ ($D_L \sim 1.7 \times 10^{28} \text{ cm}$) (Wiersema et al. 2005). The peak energy of the time-integrated spectrum obtained by Konus-wind was $E_p = 67 \pm 6 \text{ keV}$. However, the spectral indices were not available (Golenetskii et al. 2004). Therefore, method LS01 can not be used.

The γ -ray isotropic equivalent energy was $\sim 1.5 \times 10^{52}$

erg (Fan et al. 2005). The first optical observations was taken at $\sim 1000 \text{ sec}$ (Wiersema et al. 2005), which yields an upper limit of decelerating time. As the parameters are not firmly determined (Fan et al. 2005), we choose the typical parameters (with HETE-II limit: $f_{\nu,lim} \sim 1.2 \times 10^{-27} \text{ erg cm}^{-2} \text{ Hz}^{-1} \text{ s}^{-1}$). We find $\Gamma_0 < 490$ by method ZP09, and $\Gamma_0 > 120$ using SP99.

GRB 050401

GRB 050401 was located at $z = 2.9$ ($D_L \sim 7.6 \times 10^{28} \text{ cm}$). The duration of the first pulse was $\sim 6 \text{ sec}$ (De Pasquale et al. 2005). From Konus-Wind observation (Golenetskii et al. 2005a), the 2nd peak of the prompt pulses had $E_p = 119 \pm 26 \text{ keV}$, $\alpha = 0.83$, $\beta = 2.37$ and peak flux $2.45 \pm 0.12 \times 10^{-6} \text{ erg cm}^{-2} \text{ s}^{-1}$ (in the 20 keV - 2 MeV energy range). Without a direct high energy ($\sim \text{GeV}$) detection, we use method LS01B to get a lower limit. Using $f_1 \sim 0.27 \text{ cm}^{-2} \text{ s}^{-1} \text{ MeV}^{-1}$ and $\hat{\tau} \sim 1.7 \times 10^{10}$, we get $\Gamma_0 > 110$. Using the BAT limit and other typical parameters, and ZP09 we obtain $\Gamma_0 < 590$. The lower limit Rykoff et al. (2009) using method SP99 is $\Gamma_0 > 900$.

GRB 050801

GRB 050801 was located at $z = 1.56$ ($D_L \sim 3.6 \times 10^{28} \text{ cm}$). There was no observed emission at time $\sim 8 \text{ sec}$ (De Pasquale et al. 2007). The peak flux was $1.7 \pm 0.1 \text{ ph cm}^{-2} \text{ s}^{-1}$ in 15-350 keV at 1sec, and the time averaged spectral index was $\beta = 2.0 \pm 0.2$ (Sakamoto et al. 2005) (we use this as the index at the peak time). Taking the duration of the first pulse to be 2sec, we get $f_1 \sim 0.03 \text{ cm}^{-2} \text{ s}^{-1} \text{ MeV}^{-1}$, $\hat{\tau} \sim 1.5 \times 10^9$, and $\Gamma_0 > 80$ using LS01B. Giving the typical parameter values of n , ϵ_e , and ϵ_B , we get $\Gamma_0 < 420$ using ZP09. The lower limit using SP99 is $\Gamma_0 > 500$ (Rykoff et al. 2009).

GRB 050922c

GRB 050922c had $T_{90} \sim 4.5 \text{ s}$ (Sakamoto et al. 2008). It was located at $z = 2.198$ (Jakobsson et al. 2005) ($D_L \sim 5.5 \times 10^{28} \text{ cm}$), with fluence $f = 3.1 \times 10^{-6} \text{ erg cm}^{-2}$ in 30-400 keV (Crew et al. 2005), which corresponds to $E_{iso} \sim 3.7 \times 10^{52} \text{ erg}$. As the spectral power-law index was $\beta = 1.55 \pm 0.07$ (< 2) (Golenetskii et al. 2005b), we cannot use method LS01. Taking T_{90} as the duration of the first pulse and the typical parameters, we get $\Gamma_0 < 550$ using ZP09. A lower limit using method SP99 is $\Gamma_0 > 350$ (Rykoff et al. 2009).

GRB 060607a

GRB 060607a was located at $z = 3.082$ ($D_L \sim 8.2 \times 10^{28} \text{ cm}$) (Nysewander et al. 2009). With no high energy observation and a BAT photon spectral index $\beta = 1.45 \pm 0.07$ we cannot use method LS01. The first peak ended at $\sim 15 \text{ sec}$ (Ziaee pour et al. 2008). The isotropic equivalent energy was $E_{iso} \sim 1.1 \times 10^{53} \text{ erg}$. A clear optical peak was observed at $\sim 180 \text{ sec}$ (Nysewander et al. 2009). With typical parameters, the upper limit using ZP09 is $\Gamma_0 < 490$. The inferred initial Lorentz factor using SP99 is ~ 410 .

GRB 060614

GRB 060614 was located at redshift $z = 0.125$ ($D_L = 1.8 \times 10^{27} \text{ cm}$) with an isotropic equivalent energy $E_{\gamma,iso} \sim 2.5 \times 10^{51}$

ergs (Mundell et al. 2007). There was an exponential cut-off at ~ 300 keV for the intense pulse (Golenetskii et al. 2006a), which means there are practically no photons at higher energy. So we can not use method LS01. The duration of the first pulse was about 1sec (Gehrels et al. 2006). From afterglow modelling, the physical parameters are $E_k \sim 6 \times 10^{50}$ ergs, $\epsilon_e \sim 0.12$, $\epsilon_B \sim 0.0002$, and $n = 0.04 \text{cm}^{-3}$ (Xu et al. 2009). Taking the instrument limit of *Swift* BAT, we find (using ZP09) $\Gamma_0 < 530$. The peak time of the afterglow was $\sim 3 \times 10^4$ sec (Mundell et al. 2007). Taking this as the decelerating time, and $\bar{\eta} = 0.3$, we find (using SP99) $\Gamma_0 \sim 35$. This pretty low value may imply that the peak of the optical afterglow for GRB 060614 did not occur at the deceleration time but it arised due to energy injection as suggested by Xu et al. (2009).

GRB 061007

This burst was located at $z = 1.26$ ($D_L \sim 2.7 \times 10^{28}$ cm). The duration of the first pulse was ~ 3 sec (Ohno et al. 2009). The peak time was at ~ 39.5 sec, with $E_p = 498_{-48}^{+54}$ keV, $\alpha = 0.53_{-0.09}^{+0.08}$, $\beta = 2.61_{-0.25}^{+0.49}$, and the peak flux $1.95_{-0.24}^{+0.31} \text{erg cm}^{-2} \text{s}^{-1}$ (Golenetskii et al. 2006b). Taking the duration of the peak pulse to be 0.3sec (see http://gcn.gsfc.nasa.gov/notices_s/232683/BA/ for the prompt light curves), we get $f_1 \sim 3.5 \text{cm}^{-2} \text{s}^{-1} \text{MeV}^{-1}$, $\hat{\tau} \sim 6.7 \times 10^{11}$, and $\Gamma_0 > 160$ using LS01B.

The micro-physics parameters being uncertain (Mundell et al. 2007; Schady et al. 2008), we choose the normal value $\epsilon_e = 0.3$, $\epsilon_B = 0.1$ and $n = 1 \text{cm}^{-3}$, which don't affect the result much. Using the *Swift* BAT limit and equation (4), we find $\Gamma_0 \leq 480 n_0^{-1/8} \epsilon_e^{-1/6} \epsilon_B^{-1/2} \epsilon_{B,-1}^{-1/72}$ with ZP09. The optical afterglow peaked at ~ 39 sec, and the isotropic equivalent gamma-ray energy was $\sim 1.4 \times 10^{54}$ erg (Rykoff et al. 2009). We obtain, using equation (14), $\Gamma_0 \approx 640 \bar{\eta}_{-0.5}^{-1/8} n_0^{-1/8}$, which is consistent with Rykoff et al. (2009).

The later two constraints are inconsistent, and there is no much space to tune the parameters and reach consistency. However, one have to recall that method SP99 is somewhat crude and it is not clear that the inconsistency of less than a factor of 2 is significant. Moreover, a possible explanation for this contradiction could be that the Lorentz factor of the first ejected shell is less than 460, while the followed other shells move faster than the first one. After they merged, produce a single shell moving with a higher Lorentz factor. This may be an evidence that the outermost shell is accelerated during the prompt phase by other shells.

GRB 080319B

GRB 080319B, the naked eye burst, was located at redshift $z = 0.937$ (Vreeswijk et al. 2008). Its duration T_{90} was ~ 57 sec. The peak flux was $F_p \sim 2.26 \pm 0.21 \times 10^{-5} \text{erg cm}^{-2} \text{s}^{-1}$ and the peak of the νF_ν spectrum was $E_p \simeq 675 \pm 22 \text{keV}$ (i.e., $\nu_p \sim 1.6 \times 10^{20} \text{Hz}$, consequently $F_{\nu,p} \sim 1.4 \times 10^{-25} \text{erg cm}^{-2} \text{Hz}^{-1} \text{s}^{-1}$). The photon indexes below and above E_p are $0.855_{-0.014}^{+0.013}$ and $3.59_{-0.32}^{+0.62}$ respectively (Racusin et al. 2008). With luminosity distance $D \sim 1.9 \times 10^{28} \text{cm}$, GRB 080319B had a peak luminosity $L_p \sim 9.67 \times 10^{52} \text{erg s}^{-1}$ and an isotropic equivalent energy $E_{\gamma,\text{iso}} \simeq 1.32 \times 10^{54}$ erg (Golenetskii et al. 2008). The peak photon fluence is roughly $\sim 20 \text{cm}^{-2} \text{s}^{-2}$ (Racusin et al. 2008). Taking the duration of pulse ~ 2 sec, we get $f_1 \sim 2.3 \text{cm}^{-2} \text{s}^{-1} \text{MeV}^{-1}$, $\hat{\tau} \sim 3.9 \times 10^{10}$ and $\Gamma_{i,\text{min}} \sim 50$ using method LS01B. The duration of the first pulse was about 3sec, and the valley after the pulse was about 1 mJy (Racusin et al. 2008). With $A_\star = 0.01$, $\epsilon_e =$

0.2 , $\epsilon_B \sim 6 \times 10^{-7}$ (Racusin et al. 2008), we find, using ZP09, $\Gamma_0 < 580$. From the optical light curves (Pandey et al. 2009), one can estimate the deceleration time of the afterglow to be less than 100sec. Setting the efficiency parameter $\bar{\eta} = 0.3$, and the wind parameter $A_\star = 0.01$ (Racusin et al. 2008), we find, using SP99, $\Gamma_0 > 810$.

GRB 080916C

This burst was located at $z \sim 4.35$ ($D_L \sim 1.2 \times 10^{29}$ cm). To carry out method LS01, we focus on the 2nd pulse, which took place between 3.6 - 7.7sec. Two photons with energy $> 1 \text{GeV}$ were detected during this pulse. For the soft gamma-ray band, the peak energy was ~ 1170 keV, the photon spectral index in the higher band was ~ 2.21 , and the peak flux density was $3.5 \times 10^{-2} \text{cm}^{-2} \text{s}^{-1} \text{keV}^{-1}$ (Abdo et al. 2009), and then the flux at 1 MeV was $f_1 \sim 48 \text{cm}^{-2} \text{s}^{-1} \text{MeV}^{-1}$. We find $\hat{\tau} \sim 1.34 \times 10^{13}$ and $\Gamma_0 > 870$ using LS01A. This is consistent with the result of Abdo et al. (2009), while $\Gamma_0 > 490$ by method LS01B.

Consider the first pulse of this burst, which was during the period 0.004 - 3.58sec (Abdo et al. 2009). The external forward shock should not exceed the observed average gamma-ray flux $\sim 6.9 \text{cm}^{-2} \text{s}^{-1}$ (Abdo et al. 2009) in energy band 50 - 300 keV. As the photon index was ~ 0.58 , the flux density at 300 keV was $\sim 1.6 \times 10^{-26} \text{ergs cm}^{-2} \text{Hz}^{-1} \text{s}^{-1}$, which can be taken as a conservative $f_{\nu,\text{lim}}$. With typical parameters and using eq. (4), we get, using ZP09, $\Gamma_1 < 1130$. The optical afterglow showed that the deceleration time was less than 6×10^4 s (Greiner et al. 2009). With $E_{\gamma,\text{iso}} \sim 8.8 \times 10^{54}$ ergs (Abdo et al. 2009), we get the initial Lorentz factor $\Gamma_0 > 90$ using SP99.

GRB 090328A

This burst was located at $z = 0.736$ (Cenko et al. 2009) ($D_L \sim 1.4 \times 10^{28}$ cm). The spectrum from T0+3.1sec to T0+29.7sec was best fitted by a Band function with indices $\alpha = 0.93 \pm 0.02$ and $\beta = 2.2 \pm 0.1$, and peak energy of $E_{\text{peak}} = 653 \pm 45$ keV. The fluence in this time interval was $8.09 \pm 0.10 \times 10^{-5} \text{erg cm}^{-2}$ in the 8-1000 keV band and $9.5 \pm 1.0 \times 10^{-5} \text{erg cm}^{-2}$ in the 8keV-40MeV band. The isotropic equivalent energy in the 8keV-40MeV band was $E_{\gamma,\text{iso}} = 2.3 \pm 0.2 \times 10^{53}$ ergs. The 1-sec peak photon flux measured starting from T0+23.5sec in the 8-1000 keV band was $18.5 \pm 0.5 \text{ph s}^{-1} \text{cm}^{-2}$ (Rau et al. 2009a), which corresponds to $f_1 \sim 2.7 \text{ph s}^{-1} \text{cm}^{-2} \text{MeV}^{-1}$, and therefore $\hat{\tau} \sim 4.2 \times 10^{10}$ (taking the variability time scale to be 1sec). The Fermi Large Area Telescope (LAT) had detected this GRB with emission observed up to a few GeV (McEnery et al. 2009). However, the arrival time was very uncertain, even up to 900sec (Cutini et al. 2009). Here we assume the observed highest photon is 5 GeV, and it was in the same time interval of the prompt soft γ -rays. We get $\Gamma_0 \geq 320$ using LS01A and $\Gamma_0 \geq 130$ using LS01B. The first pulse was about 4.2sec (Rau et al. 2009a). By taking typical parameter, we find $\Gamma_0 < 540$ using ZP09. As the early full optical light curve is not available, we cannot carry out the SP99 method for this burst.

GRB 090424

GRB 090424 was located at $z = 0.544$ (Chornock et al. 2009) ($D_L = 9.6 \times 10^{27}$ cm). The peak energy of this burst was $E_p = 177 \pm 3$ keV, with $\alpha = 0.9 \pm 0.02$ and $\beta = 2.9 \pm 0.1$

(Connaughton et al. 2009). The 0.128-sec peak photon flux measured at 1.4sec in the 8-1000 keV band was $137 \pm 5 \text{ ph s}^{-1} \text{ cm}^{-2}$ (pulse duration $\sim 0.3 \text{ s}$) (Connaughton et al. 2009). We get $f_1 \sim 1.6 \text{ cm}^{-2} \text{ s}^{-1} \text{ MeV}^{-1}$, $\hat{\tau} \sim 4.0 \times 10^{10}$, and $\Gamma_0 \geq 70$ using LS01B. Without observations of high energy (GeV) photons, method LS01A cannot be used.

The fluence (8-1000 keV) over the entire event was $5.2 \pm 0.1 \times 10^{-5} \text{ erg cm}^{-2}$ (Connaughton et al. 2009), corresponding to the $E_{\gamma, \text{iso}} \sim 4 \times 10^{52} \text{ erg}$. We take the valley at 6sec (the first major pulse was $\sim 6 \text{ sec}$ with a few sub-pulses (Connaughton et al. 2009)) to constraint the initial Lorentz factor using ZP09. Using typical parameters, we get $\Gamma_0 \leq 300$.

The optical temporal index varied from ~ 1.2 during $\sim 100 - \sim 1000 \text{ sec}$ (Xin et al. 2009). This indicate deceleration time should be less than $\sim 100 \text{ sec}$. Using method SP99, we get the $\Gamma_0 \geq 310$.

GRB 090510

GRB 090510 was classified as short burst with a duration 0.5sec (Hoversten et al. 2009). It was located at a redshift $z = 0.903 \pm 0.003$ (Rau et al. 2009b), corresponding to a luminosity distance $1.8 \times 10^{28} \text{ cm}$. The integrated spectrum was well fitted by a Band function with $\alpha = 0.80 \pm 0.03$, $\beta = 2.6 \pm 0.3$ and $E_p = 4.4 \pm 0.4 \text{ MeV}$, and the 8 keV to 40 MeV fluence was $\sim 3.0 \times 10^{-5} \text{ erg cm}^{-2}$ (Guiriec et al. 2009), corresponding to the total isotropic equivalent energy $6.4 \times 10^{52} \text{ erg}$. The peak photon flux was $80 \text{ cm}^{-2} \text{ s}^{-1}$, corresponding to $f_{4.4} \sim 24 \text{ cm}^{-2} \text{ s}^{-1} \text{ MeV}^{-1}$ (at 4.4 MeV) and $f_1 \sim 204 \text{ cm}^{-2} \text{ s}^{-1} \text{ MeV}^{-1}$ (which is the extension from the β slope), so $\hat{\tau} \sim 5.2 \times 10^{13}$. There were > 10 photons with energy $> 1 \text{ GeV}$ during the prompt phase (Omodei et al. 2009). Using this photons and taking the duration of the sub-pulses is 0.1sec, the minimal Lorentz factor satisfies $\Gamma_0 > 960$ using LS01A and $\Gamma_0 > 340$ with LS01B. The minimal energy to annihilate the high energy photon is $E_{\text{max}, \text{an}} = (\Gamma m_e c^2)^2 / E_{\text{max}} \sim 26 \Gamma_3^2 E_{\text{max}, 10 \text{ GeV}}^{-1} \text{ MeV}$, which is well above the break point of the soft-gamma spectrum. Therefore, the photon index 2.6 can be safely used.

The first valley occurred at $\sim 0.1 \text{ sec}$. Using equation (4), we find $\Gamma_0 < 620$ using ZP09. UVOT found an optical peak at $\sim 600 \text{ sec}$ (Kuin et al. 2009). Taking this as the deceleration time of the external shock, and assuming $n = 1 \text{ cm}^{-3}$, $\bar{\eta} = 0.3$, we obtain $\Gamma_0 \sim 180$ using SP99.

The limits on the initial Lorentz factor obtained using different methods are summarized in Table 1 and depicted graphically in fig. 2. For a few bursts (GRBs 050401, 050801, 061007, 080319B, 090424, 090510) the limits are inconsistent. One may wonder if this inconsistency is problematic. First, we should realize the ‘‘initial Lorentz factor’’ for the different methods point to different objects. In the method SP99, it is the ‘‘final’’ Lorentz factor after all the sub-shell merged. In method LS01 it corresponds to the specific shell which produces the GeV photons. In our method, ZP09, it is the Lorentz factor of the first shell. It is possible that different objects have different Lorentz factors even for the same event.

Moreover, the methods that depend on different assumptions, may not be that accurate. First, all three constraints assume the relation $R = 2\Gamma_0^2 c \delta t$ to obtain the emission radius. Method SP99, assume no energy injection, and it depends on parameter such as the density n and the gamma ray efficiency $\bar{\eta}$. When using LS01, E_p should be less than $E_{\text{max}, \text{an}}$, and the high energy spectrum

Table 1. Comparison of the initial Lorentz factor constraint of different methods. The inconsistent cases are in boldface.

Burst No.	z	SP99	LS01	ZP09	medium
GRB 990123	1.60	≥ 100	$\geq 180^\ddagger$	≤ 1200	uniform
	–	≥ 130	–	≤ 410	wind-type
GRB 021004	2.32	≥ 80	a,b	≤ 210	wind-type
GRB 040924	0.858	≥ 120	a,c	≤ 490	uniform
GRB 050401	2.9	≥ 900	$\geq 110^\ddagger$	≤ 590	uniform
GRB 050801	1.56	≥ 500	$\geq 80^\ddagger$	≤ 420	uniform
GRB 050922C	2.198	≥ 350	a,b	≤ 550	uniform
GRB 060607A	3.082	~ 410	a,b	≤ 490	uniform
GRB 060614	0.125	~ 35	a,d	≤ 530	uniform
GRB 061007	1.26	~ 640	$\geq 160^\ddagger$	≤ 480	uniform
GRB 080319B	0.937	≥ 810	$\geq 50^\ddagger$	≤ 580	wind-type
GRB 080916C	4.35	≥ 90	$\geq 880^\dagger$	≤ 1130	uniform
GRB 090328A	0.736	e	$\geq 320^\dagger$	≤ 540	uniform
GRB 090424	0.544	≥ 310	$\geq 70^\ddagger$	≤ 300	uniform
GRB 090510	0.903	~ 180	$\geq 960^\dagger$	≤ 620	uniform

a. no high energy ($\sim \text{GeV}$) observations; b. photon index is less than 2; c. no photon indices; d. exponential cutoff; e. no optical data available. † limit A of LS01; ‡ limit B of LS01.

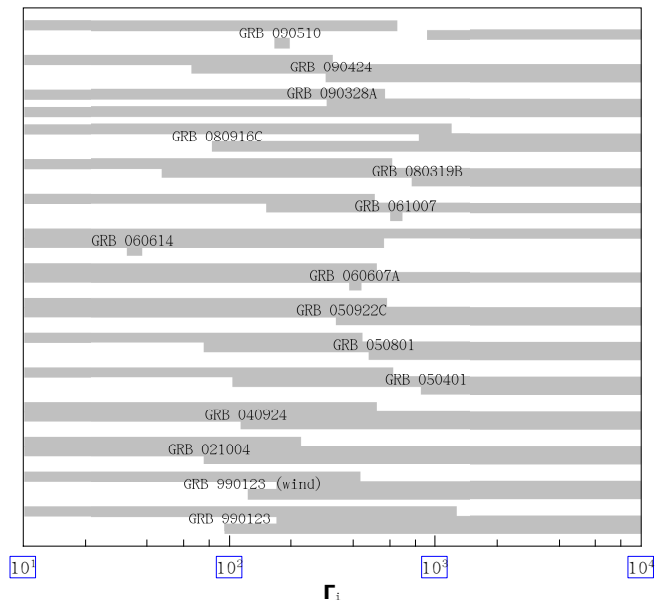


Figure 2. The allowed space (in grey) for Γ_0 for different bursts by three different methods. For each burst, from bottom up the methods are SP99, LS01 and ZP09 respectively. For the limits A and limit B in method LS01, only the higher value is used.

should obey the Band function. Finally for ZP09, particle’s power-law distribution and early formed external shock are assumed.

5 CONCLUSION AND DISCUSSION

We have considered the very early emission from the external shock, that begins to develop already during the prompt stage and emits soft γ -rays. Such emission was not identified so far. It is possible that we have seen such early soft γ -ray emission from the external shock, either as a single smooth light curve like the one observed in GRBs 911022 and 920216 (Fishman et al. 1994), or as a

smooth pulse following some additional pulses like GRB 050525A (Blustin et al. 2006) and 080916A (Ziaepour et al. 2009), or that the signal was hidden among numerous pulses like GRBs 911106 and 911127, 920221 (Fishman et al. 1994). However, one cannot confirm that these signals arose from external shocks. On the other hand, in many bursts a clear strong minima, reaching the sensitivity limit of the detector that follows the first pulse puts a very strong limits on this emission. These limits constrain the physical parameters of these GRBs and in particular the initial Lorentz factor. In cases when a clear minima is seen after the first prompt pulse this leads to a strong upper limit, typically of order of a few hundreds on the Lorentz factor. The exact value depends rather weakly on the sensitivity of the observing instrument, the distance, the density of the environment, the duration of the first γ -ray pulse and on the micro-physical parameters.

In view of the insensitivity of the constraint to various parameters, it is rather robust, provided that it is applicable and that the external shocks model is relevant at this stage. For example the very early external shock results from the interaction with matter that is rather close to the progenitor star and the environment is rather uncertain. These considerations rule out a dense r^{-2} wind profile that extends all the way to small distance from the progenitor as this would produce a too strong early external shock signal. Additionally, it applies to the Lorentz factor of the outermost shell, which could be slow relative to subsequent shells that follow.

A comparison with two other independent methods to estimate the Lorentz factor reveals that the three methods are inconsistent (by a factor of up to 1.5) in 5 out of 14 cases considered. This factor of 1.5 may not be significant taking into account the uncertainties in some of the methods. In method SP99, the Lorentz factor depends on the total kinetic energy and the environmental density, while the kinetic energy is very uncertain. In method LS01, the Lorentz factor depends sensitively on the spectral index β which is uncertain especially in the higher energy band. The assumption of a spectral single power-law in the higher energy, used in LS01B, may also be invalid. Moreover, we should notice that the different methods actually address different “initial Lorentz factors”: the “final” Lorentz factor after all the sub-shells merged (in SP99), the Lorentz factor of the shell emitting the highest energy photons (in LS01) and the Lorentz factor of the outmost shell (in ZP09).

Additional bursts, and in particular additional bursts containing GeV emission detected by Fermi for which the compactness problem is most efficiently utilized will enable us, hopefully in the near future, to confront the very early afterglow constraint with the lower limits obtained by the compactness problem. Consistency between the two will confirm that we are on the right track towards a resolution of how GRBs work, while a significant contradiction will pose yet another puzzle.

ACKNOWLEDGMENTS

We thank R. Sari, and Y. Z. Fan for the helpful discussion. This work is supported by an ERC advanced research grant and by the center of excellence in High Energy Astrophysics funded by the Israel Science Foundation by the Schwartzmann chair (TP) and by the National Natural Science Foundation of China under the grant 10703002 (fYCZ).

REFERENCES

- Abdo A. A. et al., 2009, *Science*, 323, 1688
 Achterberg A., Gallant Y. A., Kirk J. G., Guthmann A. W., 2001, *MNRAS*, 328, 393
 Baring M. G., & Harding A. K., 1997, *ApJ*, 491, 663
 Berger E., et al., 2003, *Nature*, 426, 154
 Blustin A. J., et al., 2006, *ApJ*, 637, 901
 Campana S., et al., 2006, *Nature*, 442, 1008
 Cenko S. B., et al., 2009, *GCN circular*, 9053
 Chornock R., et al., 2009, *GCN circular* 9243
 Connaughton V., et al., *GCN circular* 9230
 Crew G., et al., 2005, *GCN circular*, 4021
 Cutini S., et al., 2009, *GCN circular*, 9077
 De Pasquale M., et al., 2005, *MNRAS*, 365, 1031
 De Pasquale M., et al., 2007, *MNRAS*, 377, 1638
 Fan Y. Z., Zhang B., Kaobayashi S., Mészáros P., 2005, *ApJ*, 628, 867
 Fenimore E. E., Epstein R. I., & Ho C., 1993, *A&AS*, 97, 59
 Fishman G. J., et al., 1994, *ApJ*, 92, S229
 Fox D. W., et al., 2003, *Nature*, 422, 284
 Galama T. J., et al., 1999, *Nature*, 398, 394
 Gehrels N. et al., 2004, *ApJ*, 611, 1005
 Gehrels N. et al., 2006, *Nature*, 444, 1044
 Golenetskii S., et al., 2004, *GCN, circular*, 2754
 Golenetskii S., et al., 2005a, *GCN, circular*, 3179
 Golenetskii S., et al., 2005b, *GCN, circular*, 4030
 Golenetskii S., et al., 2006a, *GCN, circular*, 5264
 Golenetskii S., et al., 2006b, *GCN, circular*, 5722
 Golenetskii S., et al., 2008, *GCN, circular*, 7482
 Goodman J., 1986, *ApJ*, 308, L47
 Goodman J., 1997, *New Astron.*, 2, 449
 Greiner J., et al., 2009, arXiv:0902.0761
 Guiriec S., et al., 2009, *GCN circular* 9336
 Hoversten E. A., et al., 2009, *GCN circular* 9331
 Jakobsson, P., Fynbo, J. P. U., Paraficz, D., Telting, J., Jensen, B. L., Hjorth, J., & Cern, J. M. C. 2005, *GCN Circular* 4029
 Jin Z. P., Fan Y. Z., 2007, *MNRAS*, 378, 1043
 Kobayashi S., 2000, *ApJ*, 545, 807
 Kuin N. P. M., et al., 2009, *GCN circular*, 9342
 Kulkarni S. R., et al., 1999, *Nature*, 398, 389
 Panaitescu A., Kumar P., 2002, *ApJ*, 571, 779
 Lamb D., et al., 2001, *GCN Circular* 1600
 Li Z. Y., Chevalier R. A., 1999, *ApJ*, 526, 716
 Li Z. Y., Chevalier R. A., 2003, *ApJ*, 589, L69
 Lithwick Y., Sari R., 2001, *ApJ*, 555, 540
 Mangano V., et al., 2007, *A&A*, 470, 105
 McEnery J., et al., 2009, *GCN circular*, 9044
 Mészáros P., & Rees M., 1997, *ApJ*, 476, 232
 Molinari E., et al., 2007, *A&A*, 469, L13
 Mundell C. G., 2007, *ApJ*, 660, 489
 Nakar E., Piran T., 2004, *MNRAS*, 353, 647
 Nakar E., Piran T., Sari R., 2005, *ApJ*, 635, 516
 Nysewander M., Reichart D. E., Crain J. A., Foster A., Haislip J., Ivarsen K., Lacluyze A., & Trotter A., 2009, *ApJ*, 693, 1417
 Ohno M., et al., 2009, arXiv:0812.3737
 Omodei N., et al., 2009, *GCN circular*, 9350
 Oren Y., Nakar E., Piran T., 2004, *MNRAS*, 353, L35
 Panaitescu A., 2005, *ApJ*, 363, 1409
 Panaitescu A., Kumar P., 2000, *ApJ*, 543, 66
 Pandey S. B., et al., 2009, arXiv:0904.1797

- Pe'er A., Ryde F., Wijers R. A. M. J., Mészáros P., Rees M. J., 2007, *ApJ*, 664, L1
- Piran T., 1995, Proceedings of "Some Unsolved Problems in Astrophysics", Princeton, Eds. J. Bahcall and J. Ostriker (arXiv:astro-ph/9507114)
- Piran T., 2005, *Rev. Mod. Phys.*, 76, 1143
- Racusin J. L., et al., 2008, *Nature*, 455, 183
- Rau A., et al., 2009a, GCN circular, 9057
- Rau A., McBreen S., Kruehler T., Greiner J., 2009, GCN circular, 9353
- Ruderman, M., 1975, in 7th Texas Symposium on Relativistic Astrophysics, Dallas, Tx., 1974, *Ann. N.Y. Acad. Sci.* 262, 164
- Ryde F., 2005, *ApJ*, 625, L95
- Rykoff E. S. et al., 2009, arXiv:0904.0261
- Sakamoto T., et al., 2005, GCN Circular, 3730
- Sakamoto T., et al., 2008, *ApJS*, 175, 179
- Sari R., Piran T., 1995, *ApJ*, 455, L143
- Sari R., Piran T., 1999a, *ApJ*, 517, L109
- Sari R., Piran T., 1999b, *ApJ*, 520, 641
- Sari R., Piran T., Narayan R., 1998, *ApJ*, 497, L17
- Schady P., et al., 2008, *AIPC*, 1000, 200
- Taylor G. B., Frail D. A., Berger E., Kulkarni S. R., 2004, *ApJ*, 609, L1
- van Paradijs J., Kouveliotou C., & Wijers R. A. M. J., 2000, *ARA&A*, 38, 379
- Vreeswijk P. M., et al., 2008, GCN circular, 7444
- Wang X. Y., Dai Z. G., Lu T., 2000, *MNRAS*, 319, 1159
- Waxman E., Kulkarni S. R., Frail D. A., 1998, *ApJ*, 497, 288
- Wiersema K., et al., 2005, *A&A*, 481, 319
- Woods E., & Loeb A., 1995, *ApJ*, 453, 583
- Wu X. F., Dai Z. G., Huang Y. F., Lu T., 2003, *MNRAS*, 342, 1131
- Xin L. P., et al., 2009, GCN circular 9225
- Xu D., et al., 2009, *ApJ*, 696, 971
- Xue R. R., Fan Y. Z., Wei D. M., 2009, arXiv:0902.2613
- Zhang B., Fan Y. Z., Dyks J., Kobayashi S., Mészáros P., Burrows D. N., Nousek J. A., Gehrels N., 2006, *ApJ*, 642, 354
- Zhang B., Kobayashi S., Mészáros P., 2003, *ApJ*, 595, 950
- Ziaepour H., et al., 2008, *MNRAS*, 385, 453
- Ziaepour H., et al., 2009, GCN circular, 8237
- Zou Y. C., Wu X. F., Dai Z. G., 2005, *MNRAS*, 363, 93